ELSEVIER

26 July 1996

Chemical Physics Letters 257 (1996) 273–279

CHEMICAL PHYSICS LETTERS

# Cluster–surface impact dissociation of halogen molecules in large inert gas clusters

Israel Schek [a], Joshua Jortner [a], Tamar Raz [b], R.D. Levine [b]

[a] *School of Chemistry, Tel Aviv University, Ramat Aviv, Tel Aviv 69978, Israel*

[b] *The Fritz Haber Research Center for Molecular Dynamics, The Hebrew University of Jerusalem, Jerusalem 91904, Israel*

Received 26 July 1995; in final form 16 May 1996

**Abstract**

Molecular dynamics simulations of the dissociation of $I_2$ embedded in large $Ar_n$ ($n = 319, 553$) clusters, which impact at high velocities ($v = 7–15$ km $s^{-1}$) on Pt surfaces, result in information on heterogeneous and homogeneous dissociation mechanisms. A broad distribution of dissociation lifetimes is exhibited, which can be attributed to prompt and retarded heterogeneous dissociation and to prompt, retarded and outbound homogeneous dissociation events. The propagation of a microshock wave within a large cluster can be interrogated by the homogeneous dissociation of a chemical probe, with the velocity of the propagation of the dissociation front being close to the cluster impact velocity.

High-energy cluster impact on insulator, semiconductor and metal surfaces [1–13] provided hitherto unavailable conditions for the exploration of thermally driven chemical reactions under extreme conditions of high pressures (up to 1 Mbar) and temperatures (up to $10^5$ K) [1,5,9]. There are some unique features of the novel cluster impact chemistry involving the ultrashort times for energy acquisition and chemical reaction, which may occur on the timescale of the vibrational motion, and the specific role of the cluster in the energetic and steric control of activation and reactivity [9–12]. The high efficiency of the dissociation of a halogen molecule embedded in an inert gas cluster was previously attributed [10] to two distinct mechanisms, each of which can result in a higher yield of dissociation than possible for the vibrationally cold, bare molecule.

(a) The heterogeneous mechanism, where prior to dissociation the molecule reaches the surface. The heterogeneous route dominates in smaller clusters, e.g. for $I_2Ar_n$ with $n \leqslant 20$ [10,12]. The experimental results of Yasumatsu et al. [13] for the dissociation of $I_2^-$ in $I_2^-(CO_2)_n$ ($n = 1–30$) clusters were explained [12] by this mechanism, with the cluster size dependence of the dissociation process being primarily due to vibrationally assisted heterogeneous dissociation.

(b) The homogeneous mechanism, which occurs in the interior of the cluster by a molecule–cluster atom collision and where the impact is used to rapidly heat the cluster. The contribution of the homogeneous mechanism is substantial for large clusters [10,12].

Our physical picture for the existence of the two

0009-2614/96/$12.00 
*PII* S0009-2614(96)00551-9

distinct routes for cluster impact dissociation provided a quantitative description of the dependence of the dissociation yield on the cluster size, the nature of the cluster atoms and the impact velocity [9–12]. In this Letter we present new dynamic information on the homogeneous and heterogeneous dissociation mechanisms in large $I_2Ar_n$ clusters colliding with a Pt surface, which is obtained from the correlation between the dissociation distances from the surface and the dissociation times. The distribution of the lifetimes for the dissociation of the $I_2$ molecule provides a chemical method for the interrogation of the propagation of the microscopic shock wave in the cluster, revealing novel information on thermal cluster impact femtosecond chemistry [9,12].

Our molecular dynamics (MD) simulations procedures for high-energy collisions of $I_2Ar_n$ ($n$ = 553, 319) clusters ($T$ = 10 K and center of mass velocities $v$ = 5–10 km $s^{-1}$) with a realistic Pt surface (720 atoms) arranged in six layers of 120 atoms each at $T$ = 300 K were previously described [9]. The potential parameters were previously presented [9], with the Ar–Ar, Ar–Pt, Ar–I and I–Pt being described by a Lennard-Jones potential, the $I_2$ intermolecular potential being given by a Morse potential, and the Pt surface potential was represented by a many-body Gupta potential [14–18] based on the Friedel model for d-electron transition metals [17]. To account for the interaction of the metal surface with the metal bulk, we have imposed a thermalization condition on the interior of the surface metal atoms, which are coupled to a heat bath with the bulk temperature ($T$ = 300 K) [9]. The $I_2Ar_{553}$ clusters with the $I_2$ molecule located in the center of the cluster [9] were initially equilibrated at 10 K. Different trajectories were simulated with the equilibrated cluster being initially oriented at random Euler angles with respect to the surface.

Our MD simulations are restricted to the dynamics on the ground state potential surface. The role of the electronic excitations of the Ar atoms and of $Ar_2$ excimers [19] within the cluster is expected to be unimportant, provided that the total (potential and kinetic) energy per pair of Ar atoms does not exceed their nonvertical excitation energy. These nonvertical excitation energies are approximated by the crossing of the potential curves of the $Ar(^1S_0) + Ar(^1S_0)$ ground state and of the $Ar(^3P_1) + Ar(^1S_0)$ electronically excited state. These curve crossings are exhibited in the repulsive range of both the ground state and the excited state potential curves. The nonvertical electronic excitation energy of the $Ar_2^*(^3\Sigma_\mu)$ excimer is $> 13$ eV [19]. Provided that specific high-energy pair interactions are neglected, a necessary condition for ground state adiabatic dynamics is $YE_k/n < 13$ eV, where $Y \approx 0.5$ [9] is the yield of the energy deposition into the cluster and $E_k$ is the cluster impact kinetic energy. Thus $E_k/n < 26$ eV, which corresponds to the cluster impact velocity $v < 10$ km $s^{-1}$. We considered the cluster impact velocity $v < 10$ km $s^{-1}$ as the upper limit for the absence of electronic excitations and restricted our analysis to this velocity domain. In addition, the effects of electronic excitations of $I_2$ and I, as well as electron transfer from the Pt surface to the iodine, were disregarded.

Information on the heterogeneous and homogeneous cluster impact dissociation mechanisms of $I_2Ar_n$ clusters on a Pt surface was inferred from two characteristic distances of the $I_2$ molecule, the closest iodine-atom–Pt surface distance of approach $x_{MIN}$, and the closest iodine-atom–Pt surface distance $x_D$ at which dissociation occurs. $x_{MIN}$ and $x_D$ represent the perpendicular distance of the nearest iodine atom (having its parentage in an $I_2$ molecule initially embedded in the center of the cluster) from the unperturbed surface, specified by the plane which bisects the centers of the exterior Pt atoms prior to the collision. To obtain $x_D$ we characterized the dissociation event by the first passage of the I–I distance at 3.6 Å for the dissociative trajectories of $I_2$ [9].

To provide a classification of the dissociation mechanisms we introduce the characteristic distance $x_0 = r_0[(1 + a/r_0)^{1/2} + 1]$ for the spatial onset of heterogeneous dissociation, where $r_0$ = 1.7 Å is the radius of Ar and $a$ = 3.9 Å is the lattice constant of Pt, whereupon $x_0$ = 4.7 Å. The dissociation mechanisms can now be classified according to the surface approach distance and the dissociation distance (Table 1). The homogeneous dissociation mechanism (occurring by collision with an Ar atom $x_D > x_0$) and the heterogeneous dissociation mechanism (occurring by surface collision $x_D < x_0$) which were previously introduced [10], are subdivided into prompt ($x_D \approx x_{MIN}$) and retarded ($x_D > x_{MIN}$) events

Table 1
Classification of $I_2$ dissociation mechanisms in surface impact heated $Ar_n$ clusters

| Dissociation mechanism | Characteristic distances | Timescales |
|---|---|---|
| (1) heterogeneous-prompt | $x_{MIN} \approx x_D < x_0$ | $\tau(I_2) < \tau_D \leq 2\tau$ |
| (2) heterogeneous-retarded | $x_{MIN} < x_D < x_0$ | $\tau(I_2) < \tau_D \leq 2\tau$ |
| (3) homogeneous outbound-retarded | $x_{MIN} < x_0 < x_D$ | $2\tau < \tau_D < 3.5\tau$ |
| (4) homogeneous-prompt | $x_D \approx x_{MIN} > x_0$ | $\tau_D < \tau$ |
| (5) homogeneous-retarded | $x_D > x_{MIN} > x_0$ | $\tau_D < \tau$ |

(Table 1). An additional homogeneous outbound-retarded mechanism ($x_D > x_0 > x_{MIN}$) can be realized, which involves the reflection of the molecules from the surface without much internal excitation, followed by dissociation in the interior of the cluster.

Histograms of $x_D$ (Fig. 1) reveal a broad distribution with a marked fraction of homogeneous ($x_D > x_0$) events. The fraction $q$ of heterogeneous dissociation events ($x_D < x_0$) is $q = 59\%$ for $v = 10$ km s$^{-1}$ (Fig. 1) and $q = 62\%$ for $v = 7$ km s$^{-1}$. These results are in accord with our previous analysis of the velocity dependence of the dissociation yields for $I_2Ar_{553}$ on Pt [10]. The distinction between prompt and retarded dissociation is inferred from the relation between $x_D$ and $x_{MIN}$. Fig. 2 reveals the prompt dissociation branch ($x_D \approx x_{MIN}$), which corresponds to the prompt (heterogeneous and homogeneous) dissociation, and the retarded ($x_D > x_{MIN}$) dissociation events, which correspond to the heterogeneous-retarded, the homogeneous outbound-retarded and the homogeneous-retarded processes (Table 1). From the data of Fig. 2 we conclude that the majority of the retarded dissociation events correspond to the heterogeneous and the homogeneous outbound mechanisms. The contribution of the homogeneous-re-

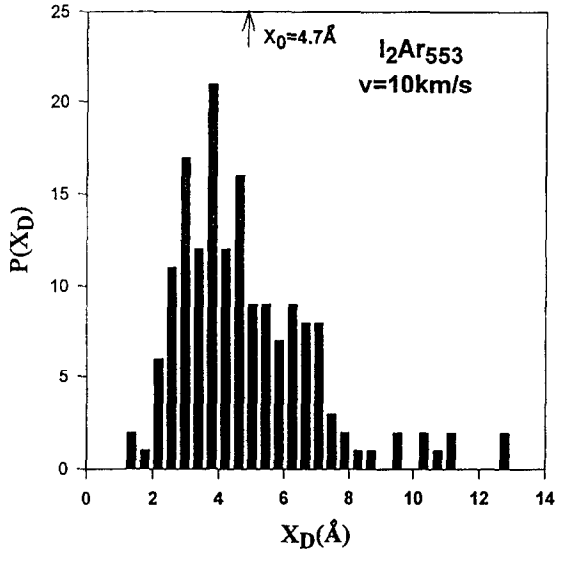


Fig. 1. A histogram for 200 trajectories of the iodine atom–(realistic) Pt surface distance ($x_D$) at which dissociation occurs (see text), computed for impact of an $I_2Ar_{553}$ cluster at $v = 10$ km s$^{-1}$.

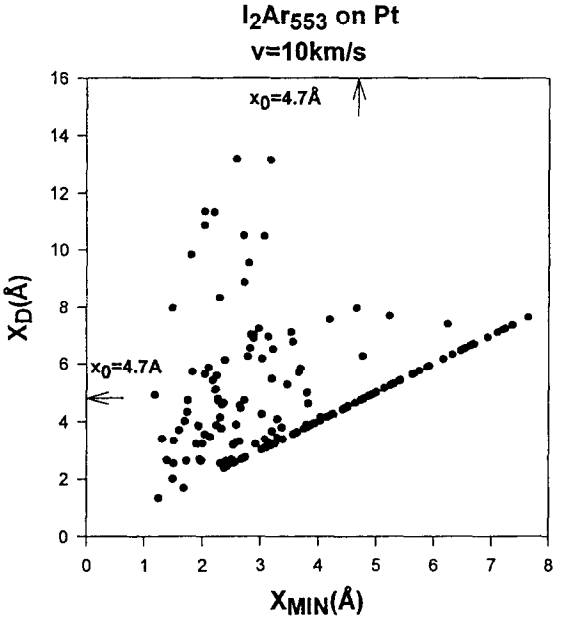


Fig. 2. The correlation between $x_{MIN}$ and $x_D$ (see text) for 200 trajectories of the impact of an $I_2Ar_{553}$ cluster at $v = 10$ km s$^{-1}$ on a Pt surface. The prompt dissociation branch represented by the linear relation $x_D = x_{MIN}$ incorporates both heterogeneous ($x_D < x_0$) and homogeneous ($x_0 > x_D$) dissociation events. The lowest left region $x_{MIN} \leq x_D < x_0$ represents prompt and retarded heterogeneous dissociation events. The upper right region $x_D \geq x_{MIN} > x_0$ represents prompt and retarded homogeneous dissociation, with the dominance of prompt events. The upper left region $x_{MIN} \leq x_0 < x_D$ represents surface assisted retarded dissociation events.

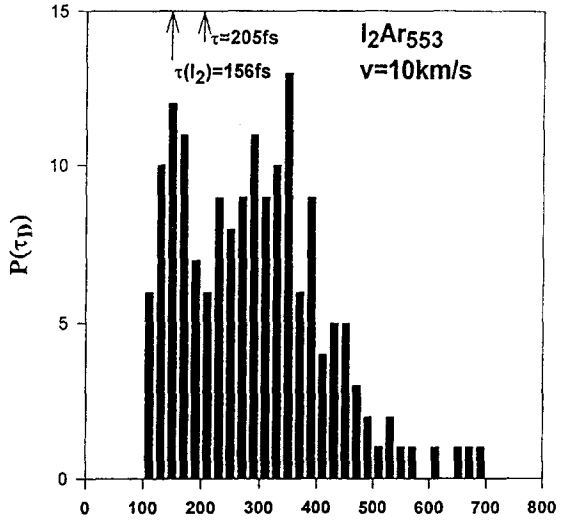


Fig. 3. A histogram for 200 trajectories of the $I_2$ dissociation times $\tau_D$ computes for the impact of $I_2Ar_{553}$ at $v = 10$ km s$^{-1}$ on a Pt surface. The distribution is bimodal, with the lowest peak around the $I_2$ vibrational time $\tau(I_2)$, while the interface between the two peaks is located at the cluster residence time $\tau$.

tarded mechanism is minor, i.e. 3% for the data of Fig. 2, and a comparable small fraction for $n = 319$; $v = 10$ km s$^{-1}$ and for $n = 553$; $v = 7$ and 15 km s$^{-1}$. Accordingly, homogeneous cluster impact dissociation is dominated by the prompt and the outbound mechanisms induced by $I_2$–Ar collisions within the cluster.

Of considerable dynamic interest is the distribution of the lifetimes $\tau_D$ for the dissociation of the $I_2$ molecules. $\tau_D$ was defined [9] for each reactive trajectory by the first passage time for the attainment of the inflexion point of the $I_2$ Morse potential (i.e. $r_e = 3.6$ Å for the I–I distance) with the origin of the timescale corresponding to the temporal onset of the cluster–wall collisions [9]. A broad distribution of dissociation times is observed, e.g. for $I_2Ar_{553}$ colliding with a Pt surface at $v = 10$ km s$^{-1}$ (Fig. 3) we obtain the lifetimes spread in the range $\tau_D = 120$–700 fs. The broad distribution of $\tau_D$ values qualitatively differs from the sharp distribution of the initial energy deposition times $t_p$ [9] from the Ar cluster to $I_2$. The $t_p$ data are interrogated by the initial sharp rise of the potential energy of the $I_2$ molecule [9]. For the $I_2Ar_{553}$ impacted on Pt at $v = 10$ km s$^{-1}$ we find $t_p = 100 \pm 10$ fs for all the trajectories. The subsequent dynamics of the impact heated cluster determines the microscopic dissociation routes. Returning to the broad distribution of $\tau_D$ values (Fig. 3) we note that the lower limit of the dissociation lifetimes is close to, but slightly lower than, the vibrational time of the $I_2$ molecule $\tau(I_2) = [c\omega(I_2)]^{-1} = 156$ fs (Fig. 3). It is instructive to establish that these dissociation events occur during the propagation of the intracluster microscopic shock wave. The timescale for the prevalence of the microscopic shock wave within $I_2Ar_n$ is determined by the cluster residence time [9] $\tau = \bar{r}_0(n+\eta)^{1/3}/v$, with $\bar{r}_0 = 2.5$ Å and $\eta = 2.9$ being the self-volume correction of $I_2$. Our previous simulations [9] also show that the timescale for the structural integrity of the cluster is $\tau_c \approx 3.0\tau$, whereupon for times exceeding $\tau_c$, cluster disintegration sets in and the intracluster microscopic shock wave dissipates. The distribution of the values of $\tau_D$ is bimodal (Fig. 3). The short $\tau_D$ subdistribution spans the range $\tau_D = 120$–200 fs $\leqslant \tau = 205$ fs, peaks around $\tau_D = \tau(I_2)$ and represents ultrashort dissociation events on the timescale $\tau_D \leqslant \tau < \tau_c$, when the cluster maintains its structural integrity. The long $\tau_D$ subdistribution spans the range $\tau_D = 200$–700 fs $\geqslant \tau = 205$ fs and peaks around $\bar{\tau} \approx 350$ fs $\approx 1.7\ \tau$, with the longer $\tau_c \approx \tau_D > \bar{\tau}$ tail of this subdistribution representing $I_2$ dissociation events just below the cluster disintegration. Finally, $\tau$ marks the interface between the short $\tau_D$ and the long $\tau_D$ subdistributions (Fig. 3). Similar features of the distribution of $\tau_D$ were obtained for other large $n = 319$ and 553 clusters at impact velocities $v = 7$–10 km s$^{-1}$. The identification of the dissociation mechanisms responsible for the bimodal distribution of $\tau_D$ (Fig. 3) is obtained from the correlation between the dissociation lifetimes $\tau_D$ and the dissociation distances (Fig. 4) and from the overview of the $x_0$–$x_{MIN}$–$\tau_D$ correlation (Fig. 5). The dissociation lifetimes reveal three distinct domains.

(1) The heterogeneous (prompt and retarded) dissociation events. These correspond to the central part of the $\tau_D$ versus $x_D$ correlation (Figs. 4 and 5) with $\tau_D = 160$–380 fs, i.e. in the range $\tau(I_2) < \tau_D < 2.0\tau$ and $x_D < x_0$ (Fig. 4 and Table 1). These dissociation lifetimes fall within the central region of the bimodal distribution of $\tau_D$ (Fig. 3) between the peaks of its two subdistributions.

(2) The homogeneous outbound-retarded dissociation events. These correspond to the upper $\tau_D$ branch

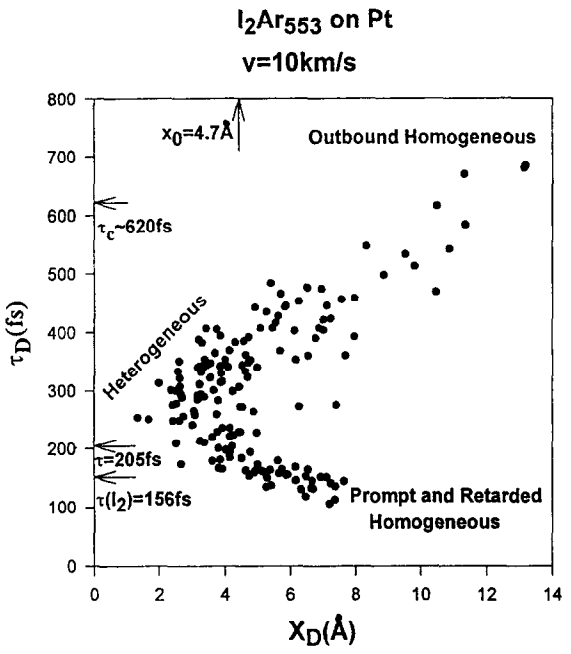


Fig. 4. The time $\tau_D$ at which the $I_2$ molecule dissociates versus the distance $x_D$ of the I atom from the surface at that instant. Computed for 200 trajectories for an $I_2Ar_{553}$ cluster impact on a Pt surface at $v = 10$ km s$^{-1}$. Marked on the figure are the characteristic times for the $I_2$ vibrational lifetimes $\tau(I_2)$, the cluster residence time $\tau$ and the time $\tau_c$ for the cluster structural integrity. The $\tau_D$ domains, which correspond to (the prompt and retarded) heterogeneous dissociation (the central part), to the prompt and retarded homogeneous dissociation (the lower branch) and to the outbound homogeneous dissociation (the upper branch) are marked on the figure.

of the $\tau_D$ versus $x_D$ correlation (Figs. 4 and 5) with $\tau_D = 400$–$700$ fs i.e. in the range $\tau_D = 2\tau$–$3.5\tau$ (Figs. 4 and 5 and Table 1). These dissociation lifetimes correspond to the long-time tail of the $\tau_D$ distribution (Fig. 3).

(3) The homogeneous (prompt and retarded) dissociation events. These correspond to the lowest branch of the $x_D$ versus $\tau_D$ correlation (Figs. 4 and 5) with $\tau_D = 160$–$120$ fs (i.e. $\tau_D \leqslant \tau(I_2)$ and $\tau_D < \tau$) with $x_D > x_0$ (Figs. 4 and 5 and Table 1). The dissociation lifetimes correspond to the short $\tau_D$ portion of the bimodal $\tau_D$ distribution (Fig. 3). These ultrashort $\tau_D (\leqslant \tau(I_2))$ homogeneous dissociation events represent $I_2$ dissociation induced via vibrational excitation by the microshock wave (i.e. $I_2$–Ar collisions within the cluster), while $I_2$ dissociation occurs during the prevalence of the shock wave ($\tau_D < \tau$).

The homogeneous-prompt and homogeneous-retarded dissociation events (dominated by the prompt

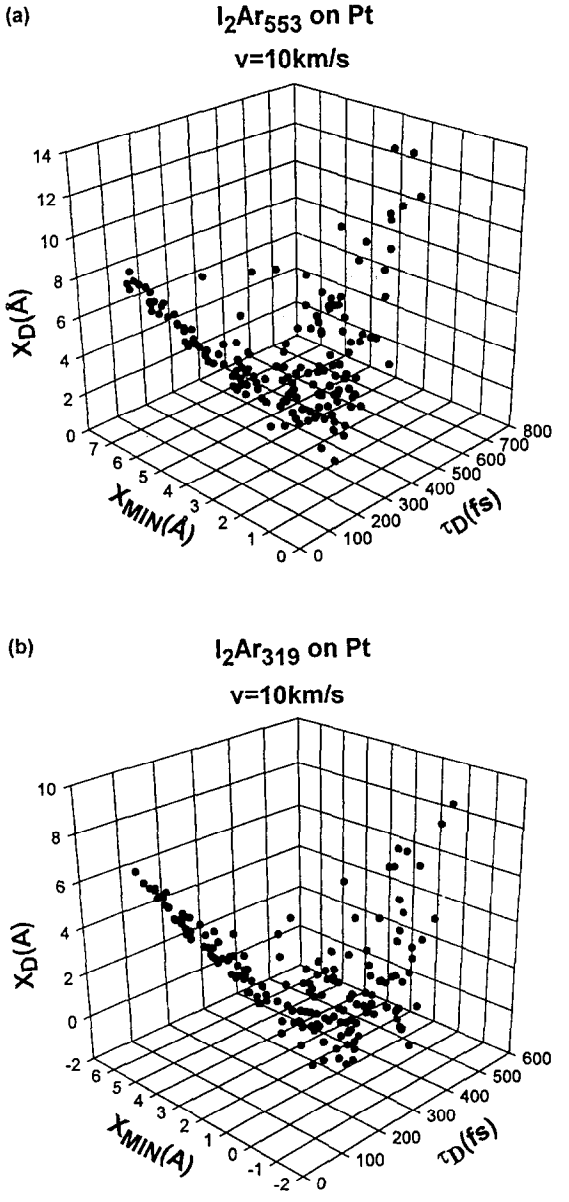


Fig. 5. The triple $x_0 - x_{MIN} - \tau_D$ correlation for 200 trajectories of $I_2Ar_n$ cluster impact dissociation at $v = 10$ km s$^{-1}$ on a Pt surface. The compression and expansion stages during the cluster impact are quite evident on these plots. (a) $n = 553$, (b) $n = 319$.

mechanism as evident from Fig. 3) constitute the shortest lifetimes for the dissociation of $I_2$ in impact excited clusters. These are characterized by bond breakage lifetimes, which are comparable to or even shorter than the vibrational lifetime $\tau(I_2) = 156$ fs of $I_2$ in its low vibrational states. This ultrafast homogeneous dissociation occurs during the propagation of the compression shock wave within the cluster. The dissociation events (4) and (5) of Table 1 constitute homogeneous dissociation during the contraction of the cluster. On the other hand, the homogeneous outbound-retarded dissociation events correspond to the longest dissociation lifetimes. This longer homogeneous dissociation occurs on the timescale of the progression of the shock wave in the cluster. The dissociation events (3) of Table 1 constitute homogeneous dissociation during the expansion of the cluster.

We propose that the propagation of the microshock wave within the large $I_2Ar_n$ cluster can be interrogated by a chemical probe, i.e. the homogeneous dissociation of $I_2$ within this cluster. This information emerges from the linear $\tau_D$ versus $x_D$ relations for the homogeneous dissociation during the cluster contraction and the cluster expansion (Figs. 4 and 5). For the homogeneous dissociation events (4) and (5) of Table 1 during the cluster contraction stage, $\tau_D$ decreases with increasing $x_D$, manifesting the transport of $I_2$ towards the surface during the cluster contraction. The linear relation between the dissociation distances and times for these homogeneous events (classes (4) and (5) of Table 1) is $\tau_D = b - ax_D$, where $b = 260$ fs and $a = 20$ fs Å$^{-1}$ for the data of Fig. 4. The velocity $u_t$ of the transport of $I_2$ towards the surface prior to its dissociation is approximately given by $u_t = a^{-1}$, resulting in $u_t = 5 \times 10^{-2}$ Å fs$^{-1}$ for $n = 553$ at $v = 10$ km s$^{-1}$. The $I_2$ transport velocity in $I_2Ar_{553}$ clusters inferred from homogeneous dissociation events (4) and (5) of Table 1 at other cluster impact velocities was found to be $u_t = 4 \times 10^{-2}$ Å fs$^{-1}$ at $v = 7$ km s$^{-1}$ and $u_t = 13 \times 10^{-2}$ Å fs$^{-1}$ at $v = 13$ km s$^{-1}$. As will be subsequently discussed $u_t$ provides an estimate for the microshock propagation velocity during the cluster contraction. For the other outbound homogeneous dissociation events (class (3) of Table 1) which occur during the cluster expansion, $\tau_D$ increases with increasing $x_D$, manifesting the displacement of $I_2$ from the surface (Fig. 4). The linear relation in this range (3) is $\tau_D = d - cx_D$ where for $n = 553$ at $v = 10$ km s$^{-1}$ (Fig. 4) $d = 200$ fs and $c = 32$ fs Å$^{-1}$. The cluster expansion velocity $u_e = c^{-1} = 3 \times 10^{-2}$ Å fs$^{-1}$ is somewhat lower (i.e. by 50%) than $u_t$. This is only to be expected in view of the considerable dissipation of energy at the Pt surface [9,10].

An alternative approach to the estimate of the microshock propagation velocity rests on geometrical information. The most distant (prompt and retarded) homogeneous dissociation event during the cluster contraction is characterized by $(x_D^0, \tau_D^0)$, where $x_D^0$ is the largest value of $x_D$ and $\tau_D^0$ is the dissociation time at $x_D^0$ in the lower branch in Fig. 4. We shall define the velocity $u_D$ for the propagation of the dissociation front within the cluster during its contraction by $u_D = x_D^0/\tau_D^0$. This analysis for homogeneous dissociation of the $I_2Ar_n$ ($n = 553$, 319) clusters resulted in $u_D = 5.5 \times 10^{-2}$ Å fs$^{-1}$ for $n = 553$ and $v = 7$ km s$^{-1}$, $u_D = 6.6 \times 10^{-2}$ Å fs$^{-1}$ for $n = 553$ and $v = 10$ km s$^{-1}$ and $u_D = 6.5$ Å fs$^{-1}$ for $n = 319$ and $v = 10$ km s$^{-1}$. Within the accuracy range of these estimates ($\pm 10\%$), $x_D^0$ at fixed $v$ decreases with decreasing $n$, i.e. for $v = 10$ km s$^{-1}$, $x_D^0 = 7.7$ Å for $n = 553$ and $x_D^0 = 6.3$ Å for $n = 319$, exhibiting an approximate $n^{1/3}$ cluster size dependence, i.e. $x_D^0 \propto R_c$, where $R_c$ is the cluster radius. $u_D$ at fixed $v$ is independent of the cluster size for large clusters. $u_D$ increases with increasing the cluster impact velocity, as expected. Finally, we note that the velocities at the dissociation front are only slightly higher (i.e. by $\approx 20\%$) than the corresponding transport velocities $u_t$ of $I_2$.

Of considerable interest is the quantification of the propagation velocity $u_s$ of the microshock wave during the cluster contraction. The velocity $u_D$ of the dissociation front represents a lower limit for $u_s$. Accordingly, from our simulation results $v/u_D = 1.4 \pm 0.2$, we infer that $v/u_s < 1.4 \pm 0.2$ for $I_2Ar_{553}$ in the cluster impact velocity range $v = 7$–$10$ km s$^{-1}$. We conclude that the velocity of the microshock wave propagation within the cluster is close to the cluster impact velocity. This estimate for the propagation velocity of the microshock wave within the large cluster can be confronted with the results of the theory of shock compression in a macroscopic material [20,21]. For a one-dimensional shock propaga-

tion at the velocity $U_s$, which is induced by a piston with the velocity $U_p$ within a macroscopic material at thermodynamics equilibrium [21], the conservation of mass, momentum and energy yields the Hugonoit equation [20,21]. Mass conservation results in the relation between the shock velocity and the piston velocity in the form [20,21] $U_p/U_s = 1 - \rho_0/\rho_1$, where $\rho_0$ is the initial density of the material and $\rho_1$ is the final density during the shock wave. Attempting a heuristic bridging between shock propagation in the cluster and in the bulk, we identify the cluster impact velocity with the piston velocity, i.e. $U_p \approx v$, and the velocity of the inward propagation of the microshock wave within the cluster with the shock propagation velocity in a macroscopic material, i.e. $U_s \approx u_s$. We also bear in mind that $\rho_0/\rho_1 \ll 1$. Accordingly, we expect that $U_p/U_s \approx v/u_s \approx 1$. This conclusion concurs with the results of the chemical interrogation of the propagation of the homogeneous dissociation front within the cluster.

The dynamics of cluster–surface impact homogeneous dissociation of a diatomic molecule in large inert gas clusters manifests an ultrafast chemical process on the timescale of intermolecular vibrational motion. The utilization of femtosecond lasers provided a powerful tool for the interrogation of ultrafast bond breaking and bond formation [22]. Homogeneous cluster impact dynamics opens up a new area of thermal femtosecond chemistry.

We are grateful to Professor K.L. Kompa for illuminating discussions. This work was supported by the German–Israel James Franck Binational Program. The Fritz Haber Research Center is supported by the Minerva Gesellschaft für die Forschung, mbH, Munich, Germany.

## References

[1] R.J. Beuhler and L. Friedman, Chem. Rev. 86 (1986) 521.
[2] U. Even, P. de Lange, H. Jonkman and J. Kommandeur, Phys. Rev. Letters 56 (1986) 956.
[3] P.M. St. John, R.D. Beck and R.L. Whetten, Phys. Rev. Letters 69 (1992) 1467.
[4] P.M. St. John and R.L. Whetten, J. Phys. Chem. 98 (1992) 3527.
[5] C.L. Cleveland and U. Landman, Science 257 (1992) 355.
[6] H. Haberland, Z. Isepov and M. Moeseler, Z. Physik D 26 (1993) 229.
[7] U. Even, I. Schek and J. Jortner, Chem. Phys. Letters 202 (1993) 303.
[8] H.P. Cheng and U. Landman, J. Phys. Chem. 98 (1994) 3527.
[9] I. Schek, T. Raz, R.D. Levine and J. Jortner, J. Chem. Phys. 101 (1994) 8596.
[10] T. Raz, I. Schek, M. Ben Nun, U. Even, J. Jortner and R.D. Levine, J. Chem. Phys. 101 (1994) 8606.
[11] T. Raz and R.D. Levine, J. Am. Chem. Soc. 116 (1994) 11167.
[12] T. Raz, I. Schek, J. Jortner and R.D. Levine, Proceedings of the Yamada Conference (1995), in press.
[13] H. Yasumatsu, T. Tsukuda, T. Sugai, A. Terasaki, T. Nataga and T. Kondow, Surface Sci. Letters.
[14] R. Gupta, Phys. Rev. B 23 (1981) 6265.
[15] G. Allen, Surface Sci 89 (1979) 142.
[16] F. Ducastelle, J. Phys. (Paris) 31 (1970) 1055.
[17] J. Friedel, in: The physics of metals, ed. J.M. Ziman (Cambridge Univ. Press, Cambridge, 1969).
[18] D. Tomanek, A.A. Aligia and C.A. Balsiero, Phys. Rev. B 32 (1985) 5051.
[19] N. Schwentner, E.E. Koch and J. Jortner, Electronic excitations in condensed rare gases (Springer, Heidelberg, 1985).
[20] Ya.B. Zeldovich and Yu.P. Raizer, Physics of shock waves and high-temperature hydrodynamics phenomena (Academic Press, New York, 1966).
[21] M. Ross, in: High pressure chemistry and biochemistry, eds. R. van Eldik and J. Jonas (Reidel, Dordrecht, 1987) p. 9.
[22] A.H. Zewail, Femtochemistry (World Scientific, Singapore, 1994).